Supplement Material

Linking chemical composition and optical properties of biomass burning aerosols in Amazonia

Milena Ponczek[1], Marco A.M. Franco[1], Samara Carbone[2], Luciana V. Rizzo[3], Djacinto Santos Junior[1], Fernando G. Morais[1], Alejandro Duarte [4], Henrique M. J. Barbosa[1], Paulo Artaxo[1].

1 Institute of Physics, University of São Paulo, Rua do Matão, Travessa R, 187, 05508-900, São Paulo, SP, Brazil
2 Institute of Agrarian Sciences Federal University of Uberlandia (UFU), Av. Amazonas, 38405-302, Uberlandia, MG, Brazil
3 Federal University of São Paulo, Av. Conceição, 329, 09920-000, Diadema, SP, Brazil.
4 Federal University of Acre, BR. 364 km 4, Distrito Industrial, 69915-900 - Rio Branco, AC, Brazil

1. Temperature, RH and pressure
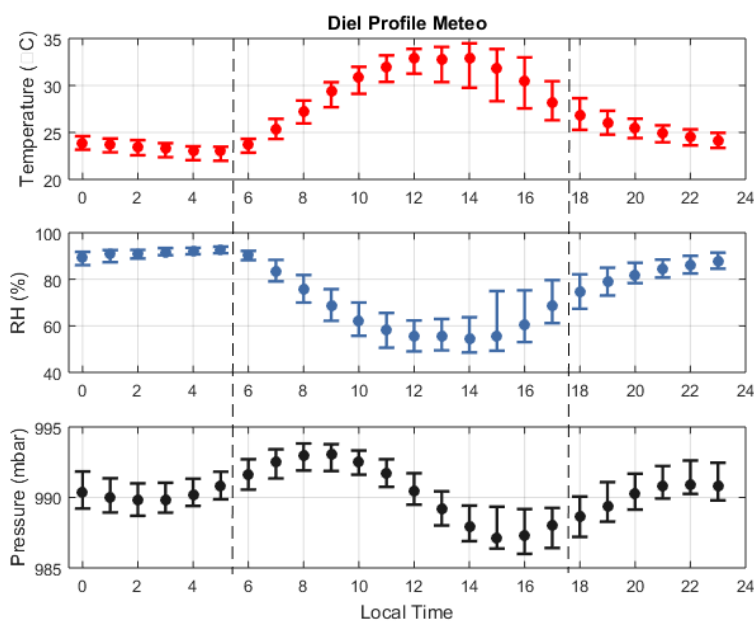
Figure SI 1: Temperature, RH and atmospheric pressure diurnal profiles

2. Trace gases - O_3, VOCs and NO_2

The diurnal profiles of the trace gases indicate strong atmospheric photochemical activity, reaching its maximum during the middle of the day when there is more intense solar radiation and

higher temperatures. The median diurnal concentrations of O_3, VOCs, and NO_2 are shown in Figure SI 2.

All the VOCs presented clear daytime patterns showing maximum values in the middle of the day. Isoprene, acetone, acetaldehyde have a maximum around 12h (LT) while methyl vinyl ketone + methacrolein (MVK+MACR) and methyl ethyl ketone (MEK) reach a maximum slightly after, 13-14h (LT). Other VOCs, usually of anthropogenic origin, such as benzene, toluene, and other aromatics, had concentrations below 0.5 ppb and a flat and undefined diurnal profile (not shown). Acetaldehyde and acetone (as well as MACR, MVK, MEK recognized isoprene oxidation products) have their daytime profiles correlated, indicating that both emission and photochemical production would be associated with biogenic processes. Therefore, the VOCs presented in Figure SI 2 were grouped as biogenic (BVOCs). Profiles and absolute concentration values of BVOCs are close to those reported by Yañez-Serrano et al (2015) [1] for the dry season in Central Amazonia, when for instance, daytime isoprene reached 2-3 ppb (median) at the ground between 12:00–15:00 LT.
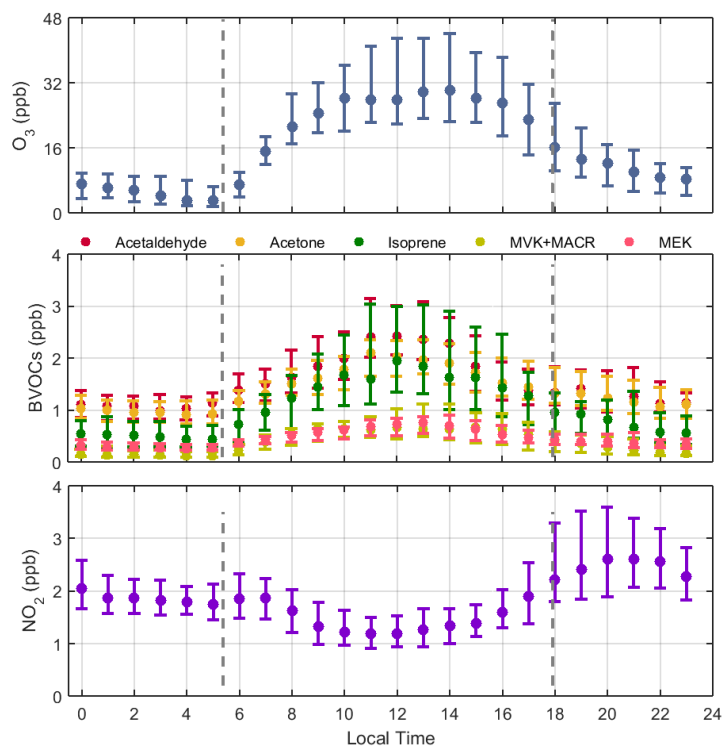
Figure SI 2: Diurnal variations of O_3, BVOCs and NO_2, concentrations. Points are median values and error bars indicate 25 and 75% percentiles. The dashed vertical bars represent the sunrise and sunset times, respectively.

Trace gases (O_3 and NO_2) diel patterns are similar to those reported at a pasture site in Southwestern Amazonia (Rondônia) in 1999 [2], considering daytime variability and concentration ranges. In Rio Branco, the maximum average ozone concentration was approximately 32 ppb at 13-14h (LT) and coincided with the NO_2 minimum of approx. 1 ppb, while at Rondônia Pasture Site maximum O_3 and minimum NO_2 were around 50 ppb and 2 ppb, respectively. As a matter of comparison, at Manaus city vicinities during the wet-to-dry transition, daytime O_3 mixing ratios for days with low influence from the city plume were on average 21 ppb, meanwhile for the polluted days were on average 31 ppb with maximal values of 60 ppb [3,4]. These high O_3 concentrations produced by biomass burning could be damaging the forest [5].

3. PM1 mass closure
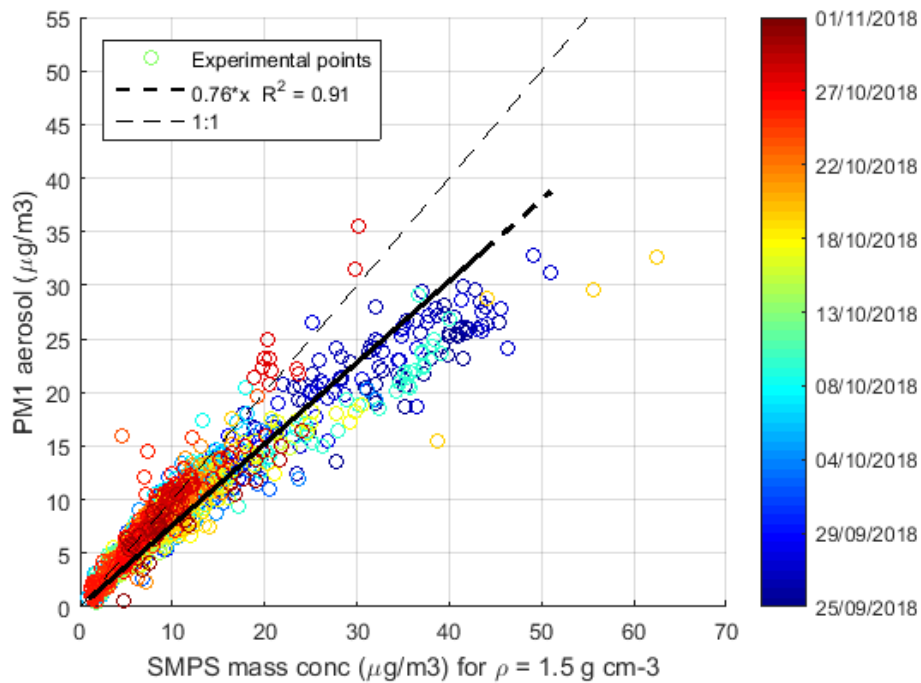
Figure SI 3: Scatter plot between PM1 (PM1 = NR-PM1 + BCe) and SMPS-PM1 (PM1 mass concentration estimated using particle size distribution assuming particle density of 1.5 g cm−3 as reported by Britto et al, (2014)[6]).

4. Air masses back trajectories x fires spots

The number of fire outbreaks (FRP, precipitation, temperature, radiation, etc.) was counted in an area of 100 x 100 km around each point of the trajectory, as in Figure SI *4*. Thus, only the fires that were active at the moment the trajectory passes over that region were considered.
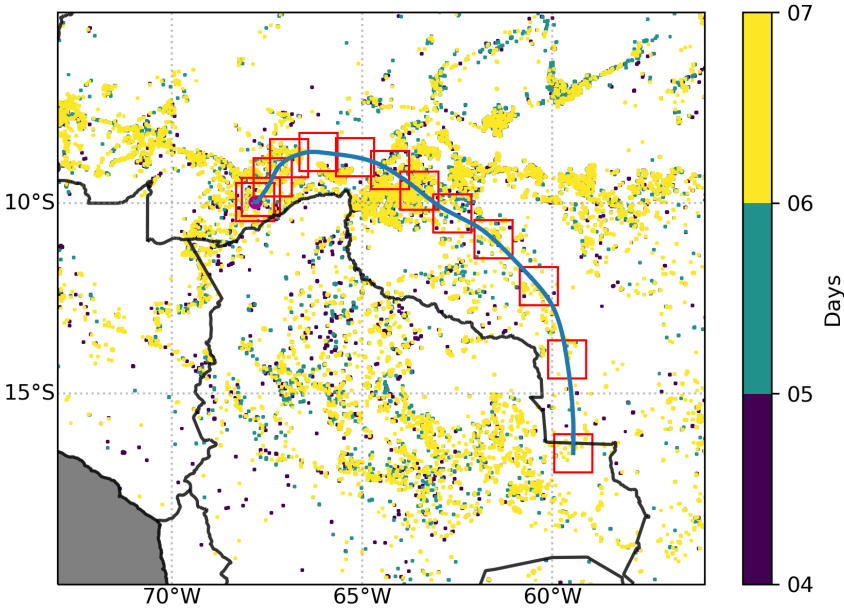
Figure SI 4: Counting of fires spots around the back-trajectory for the days 5-7 September 2018. The color bar represents the day when the fire focus was active. The red square is the area around the trajectory point used for the integration of meteorological variables.

Applying the method for all trajectories for each period (period 1 and period 2) of the campaign, we compare the median of the sum of fires (in number) and the Fire Radiative Power (in W/m²) that cross the trajectories in each period, Figure SI *5*.
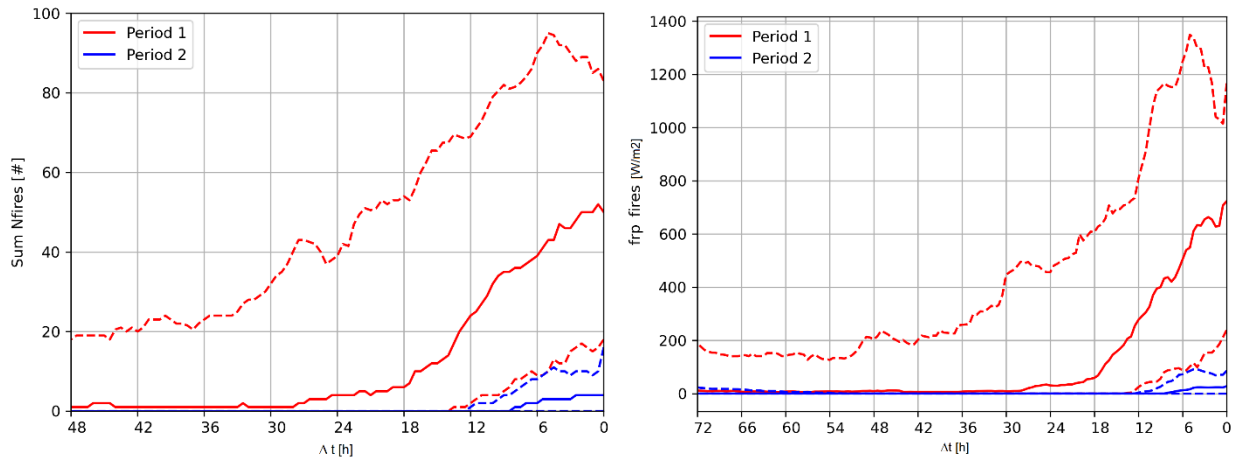
Figure SI 5: a) Sum of fire outbreaks and b) Sum of Fire Radiative Power (FRP) that cross the back-trajectories, during each period. The x-axis corresponds to the duration (Δt) of the back trajectories, where 0 is the moment when the trajectory arrived at the site. Full lines are the median and dashed lines are 25 and 75 quartiles. For period 1, 1823 trajectories were accounted, and 1176 for period 2, with each trajectory from 48 h backwards being composed of 96 coordinate points.

We can also note that the number of fires and the Fire Radiative Power (FRP) give similar results. Therefore, both variables represent well the fires incidence in the region.

To further investigate the influence of biomass burning on aerosol composition, the same methodology was applied accounting for selected trajectories when a 'flag' was activated according to thresholds indicating, for example, high PM1 concentration, or BrC fraction. Upper and lower thresholds were established to filter the periods in which the selected variables were above or below these values which were determined considering the percentiles of each parameter (95th vs 5th for upper and lower, respectively) resulting in a similar number of points that meets the condition, as shown in Table SI 1. Figure SI 6 shows the periods when each flag was activated, for both upper and lower conditions.

Table SI 1: Variables and their respective upper and lower thresholds. In parentheses the number of points meeting each condition

Parameter	Upper Threshold	Lower Threshold
PM1 concentration (µg m^{-3})	≥ 24.8 (211)	≤ 4.5 (193)
f60/f44	≥ 0.044 (144)	≤ 0.01 (120)
BrC fraction	≥ 27% (74)	≤ 14% (118)
Massive BB	from 09/07 to 09/12/2018	
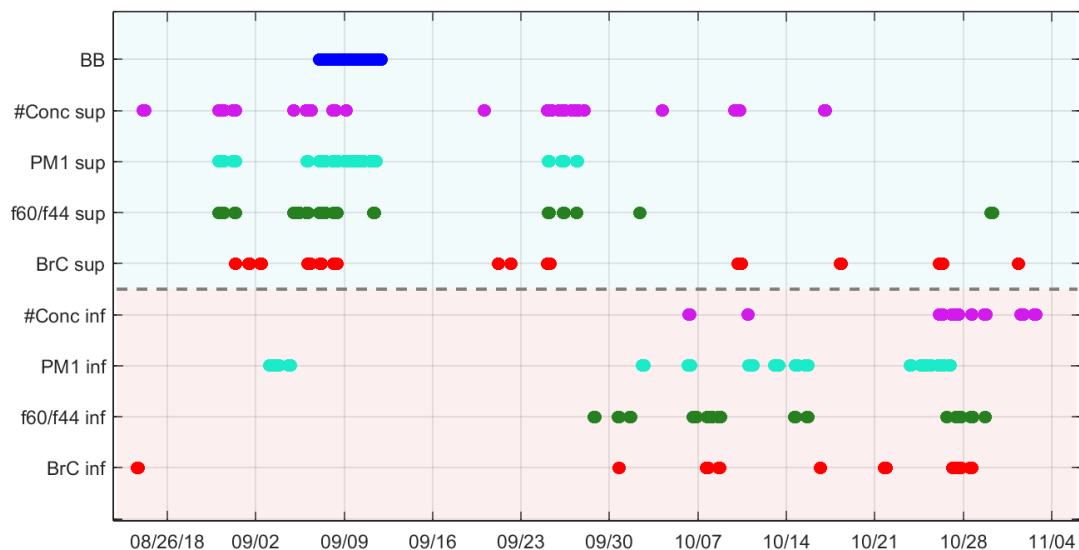
Figure SI 6: Periods when each flag was activated, for both upper and lower thresholds.

The analysis of the trajectories filtered by the pre-established flags helped in the interpretation of the results showing that when high fractions of BrC and f60 / f44 were measured on the site, the air masses came from a path with more fire spots, less precipitation, and higher altitudes, as shown in Figure SI 7.
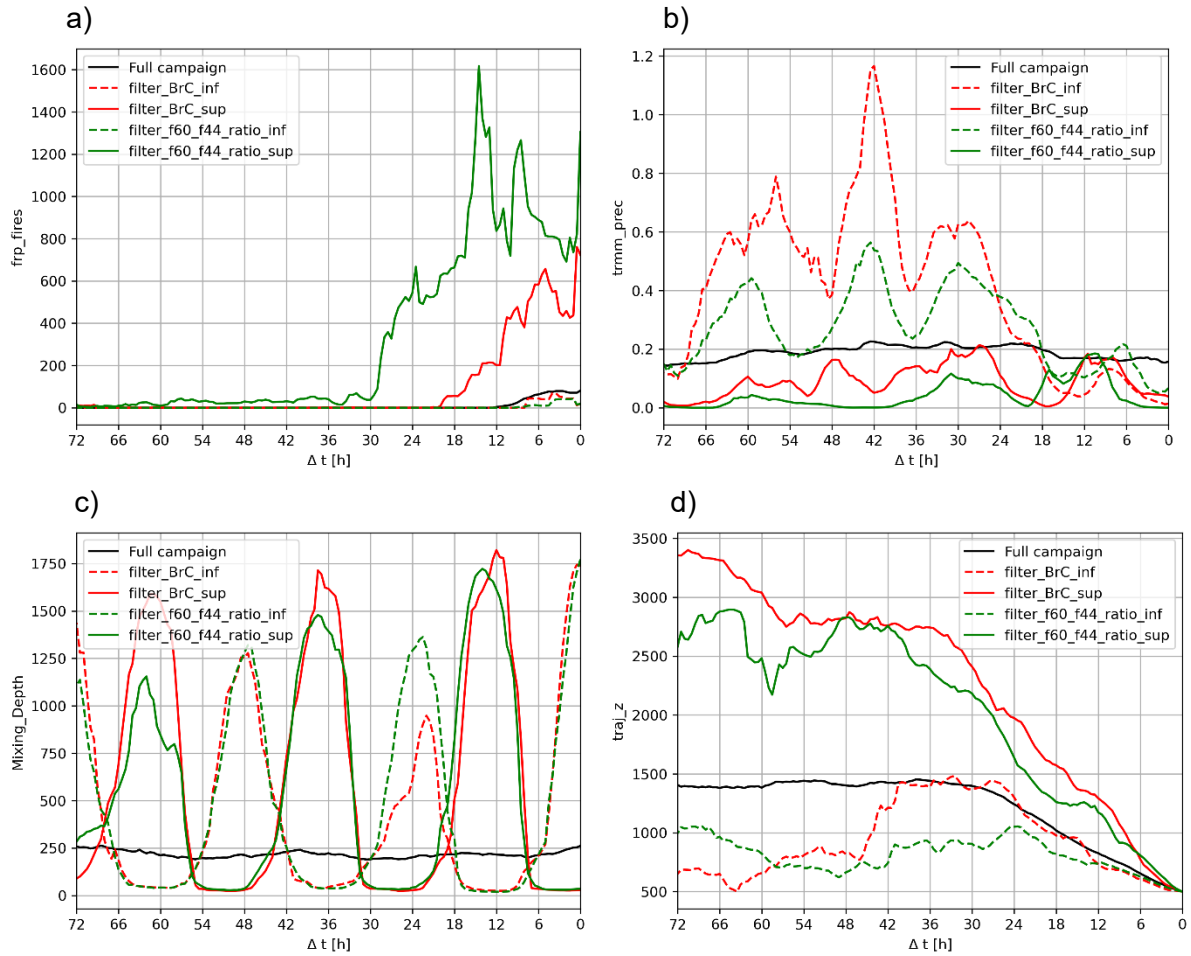
Figure SI 7: a) Median of the sum of Fire Radiative Power (FRP) b) Median precipitation (mm) c) Median mixing depth height and d) Median trajectory height for selected back-trajectories when the flags BrC inf, BrC sup, f60/f44 inf and f60/f44 sup were activated (according to Figure SI 6 and Table SI 1). Similar do Figure SI 5, the x-axis corresponds to the duration (Δt) of the back trajectories, where 0 is the moment when the trajectory arrived at the site. Full lines are the median and dashed lines are 25 and 75 quartiles. The number of trajectories that were accounted for each flag is indicated in Table SI 1.

5. Aeronet BrC fraction from 2000-2017
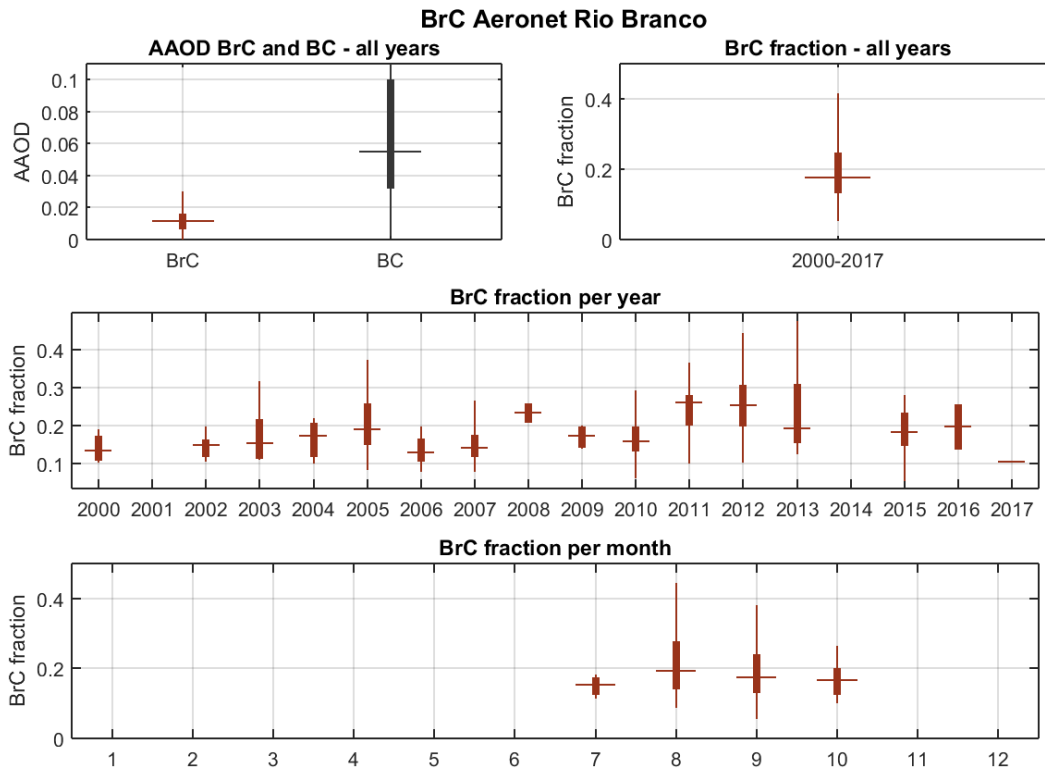
Figure SI 8: Boxplots for the BrC absorption retrieved from Aeronet for Rio Branco from 2000 to 2017. a) AAOD for BrC and BC, b) BrC fraction considering all years data coverage, c) the BrC fraction per year adn d) BrC fraction monthly statistics from 2000 to 2017. The central line mark indicates the median, and the bottom and top edges of the box, the 25th and 75th percentiles. The whiskers extend represent extreme data points not considered outliers.

6. PMF

Criteria for choosing factor number in NMR factor analysis.
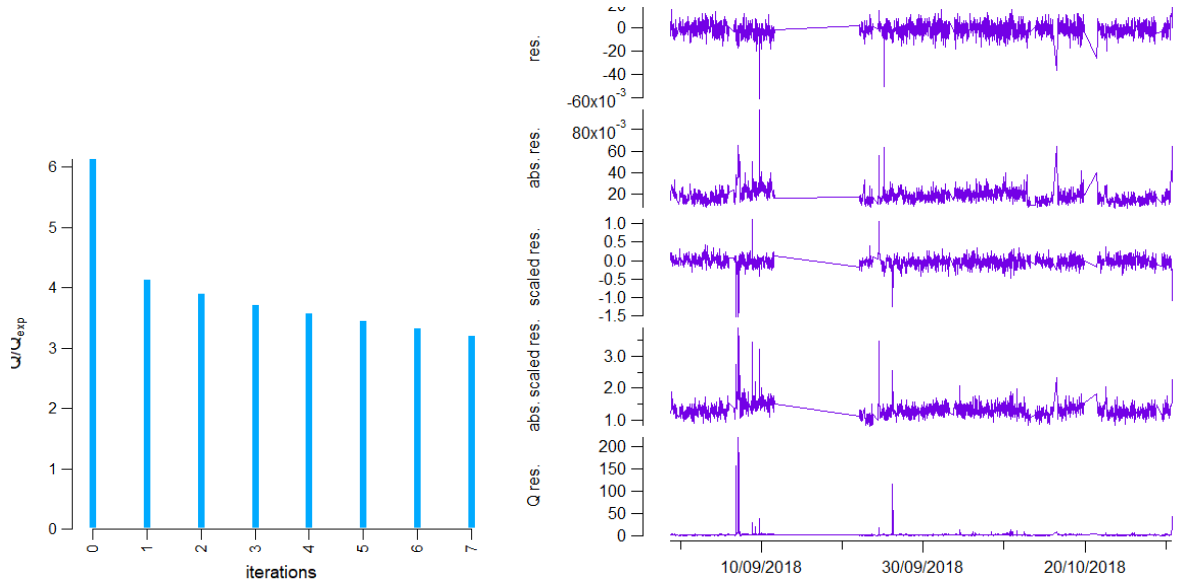
Figure SI 9: a) Q/Qexpected versus the number of factors. We choose solution (p=4). b) Time series of the model residuals for the PMF analysis.

7. Diurnal profiles PM1
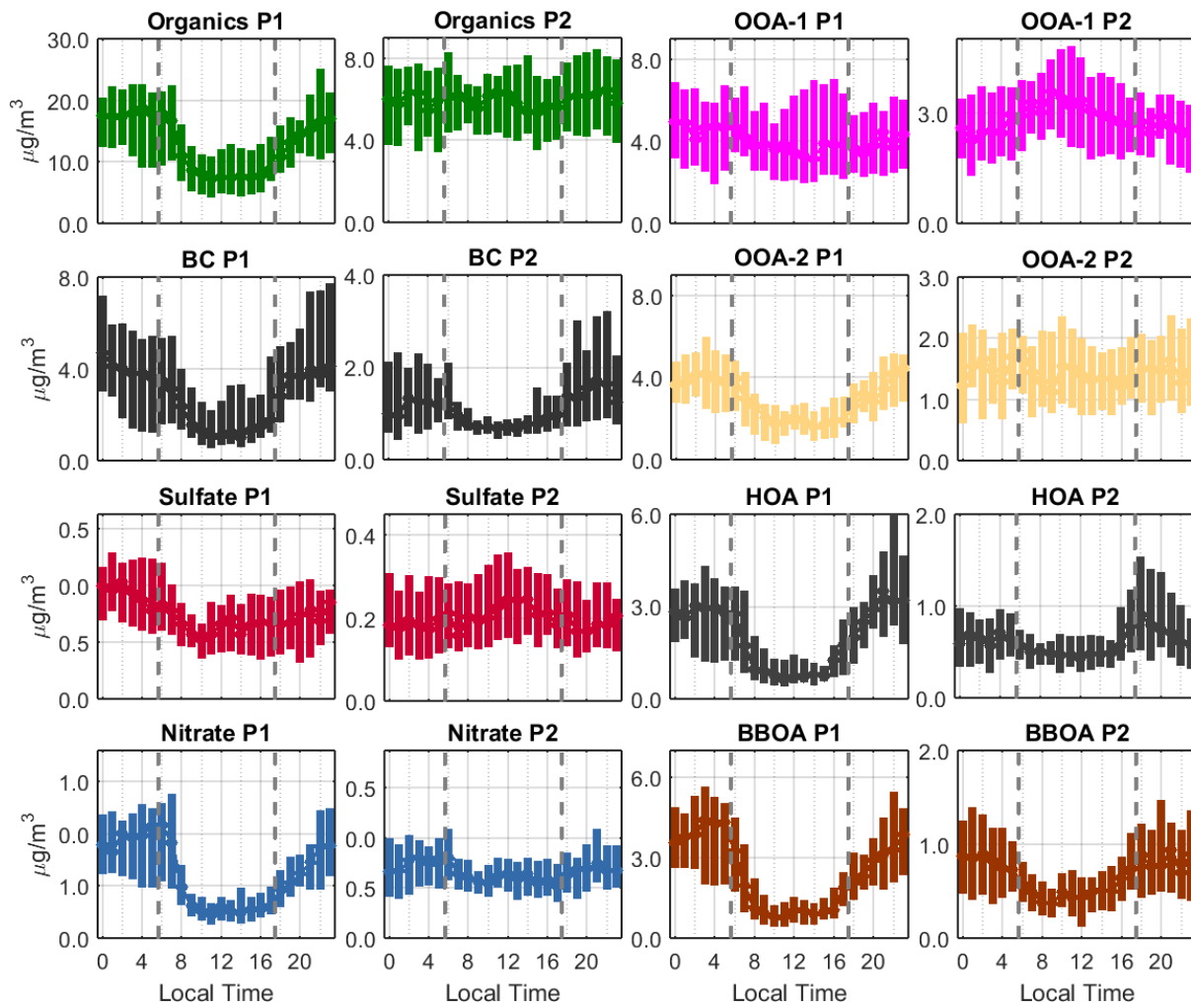
Figure SI 10: Diurnal profiles for PM1 components and PMF factors concentration in µg m-3. Points are the median values, and bars are the 1st and 3rd quartiles. Local time is UTC minus five hours. Dashed lines are a guide for sunrise and sunset time.

8. Optical Properties time series
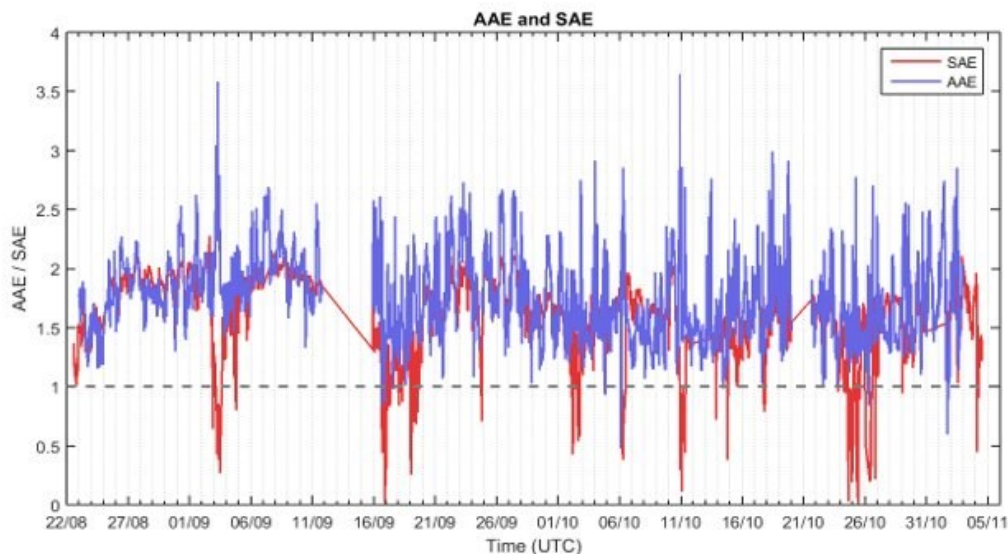
Figure SI 11: Absorption Angstrom exponent and Scattering Angstrom exponent time series for the whole campaign.

9. PM1 and OA PMF components mass concentrations and optical properties descriptive statistics

Table SI 2: Summary of PM1 and OA PMF components mass concentrations and descriptive statistics comparing the first and the second periods of the campaign. All values are given in µg m-3, unless stated otherwise.

		PERIOD 1					PERIOD 2				
		Mean	Std	Max	Median	IQR	Mean	Std	Max	Median	IQR
PM1	Organics	13.89	9.70	79.03	12.38	7.40-18.04	6.12	2.93	27.28	5.94	4.22-7.51
	Sulfate	0.31	0.17	1.04	0.30	0.19-0.40	0.22	0.13	0.80	0.19	0.12-0.30
	Nitrate	0.67	0.59	4.59	0.50	0.28-0.90	0.28	0.16	1.33	0.26	0.18-0.35
	Ammonium	0.39	0.33	2.87	0.35	0.17-0.59	0.20	0.25	1.62	0.20	0.05-0.36
	Chl	0.10	0.14	1.22	0.05	0.02-0.11	0.04	0.13	3.04	0.03	0.01-0.05
	BC	3.44	2.81	21.23	3.00	1.21-4.72	1.44	1.53	17.80	0.94	0.61-1.72
	PM1	18.80	13.01	98.28	16.74	9.61-25.26	8.31	4.27	35.48	7.83	5.55-10.25
	NR PM1	15.36	10.70	87.28	13.45	8.20-19.96	6.86	3.28	29.43	6.68	4.73-8.45
PMF	OOA-1	4.38	2.44	12.08	4.04	2.45-6.08	2.89	1.49	13.68	2.79	1.83-3.80
	OOA-2	3.24	2.72	24.25	2.77	1.60-4.18	1.51	0.93	7.31	1.44	0.89-2.07
	HOA	2.45	2.61	18.49	1.72	0.78-3.10	0.71	0.55	5.47	0.58	0.37-0.86
	BBOA	2.73	2.85	25.77	1.94	0.91-3.81	0.77	0.67	4.70	0.63	0.35-1.00
	# conc (cm^{-3})	5924	3472	18476	5056	3135-7917	4259	2762	22637	3686	2142-5618
	Dpg (nm)	-	-	-	-	-	79.87	19.22	153.10	77.58	66-92

G A S	NO$_2$ (ppm)	2.01	1.17	10.61	1.79	1.31-2.36	1.97	1.17	11.77	1.77	1.30-2.29
	O$_3$ (ppm)	20.18	16.64	81.33	16.14	6.74-30.62	15.12	10.13	53.41	13.965	7.01-21.42

Table SI 3: Summary of aerosol absorption, scattering coefficients at different wavelengths and descriptive statistics for period 1 and 2 in Rio Branco.

		PERIOD 1				PERIOD 2			
	λ	Mean +/- Std	Max	Median	IQR	Mean +/- Std	Max	Median	IQR
σ_{abs} (Mm^{-1})	370 nm	48±40	305	37	16-69	19±20	255.	12	7-23
	470 nm	28±22	176	22	11-40	12±13	172	8	4-14
	520 nm	21±17	138	17	8-30	10±10	139	6	3-12
	637 nm	15±12	112	12	6-21	7±8	101	4	2-8
	880 nm	9±7	77	7	3-12	4±5	62	3	1-5
σ_{scat} (Mm^{-1})	450 nm	81±57	387	70	35-115	42±30	314	37	23-51
	532 nm	59±41	274	50	26-83	30±22	218	27	16-37
	637 nm	43±28	185	36	20-59	23±15	146	21	13-28

10.   Average Mass Scattering Efficiencies (MSE) and Mass absorption efficiencies (MAE) estimation for multiple wavelengths
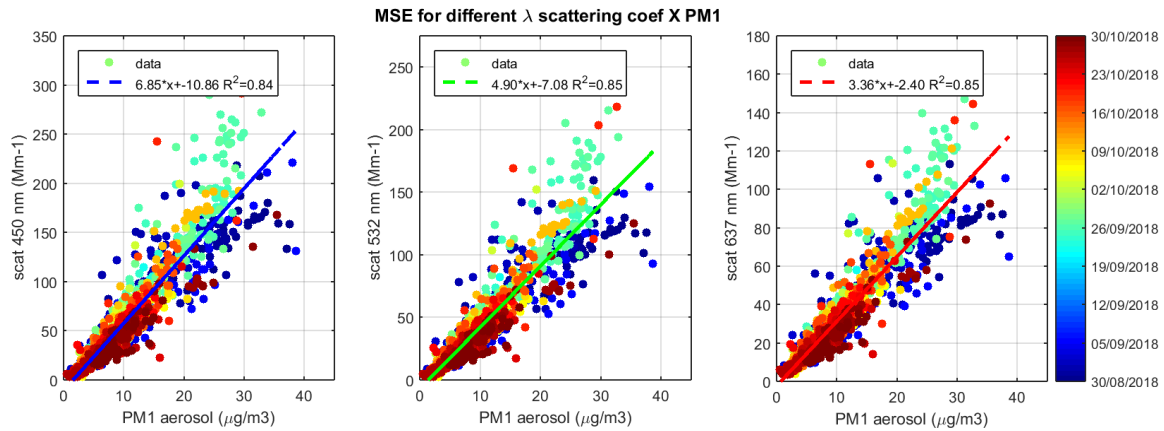
Figure SI 12: Scattering coefficient versus PM1 mass concentration for a) 450 nm, b) 532 nm and c) 637 nm. The angular coefficient from this linear regression corresponds to the mass scattering efficiency.
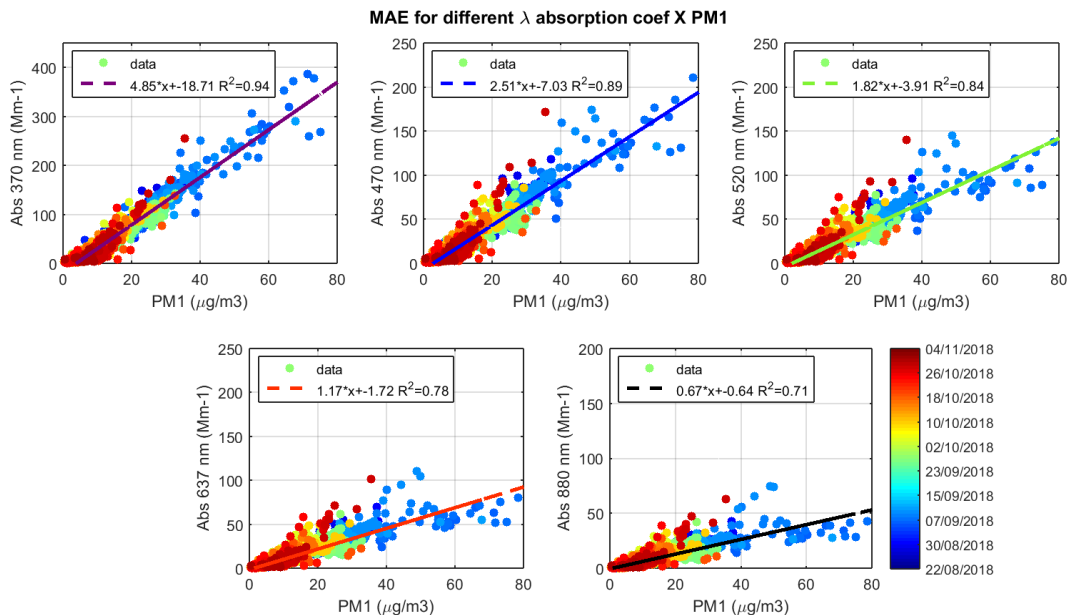
Figure SI 13: Absorption coefficient versus PM1 mass concentration for a) 370 nm b) 470 nm, c) 520 nm d) 637 nm and e) 880 nm. The angular coefficient from this linear regression corresponds to the mass absorption efficiency.

11.   Multivariate linear regression (MLR)

p-values

Table SI 4: Scattering coefficient multivariate regression p-values

	OOA-1	OOA-2	BBOA	BC	intercept
450 nm	1.61E-68	1.07E-23	1.84E-90	5.44E-101	8.33E-5
532 nm	8.33E-98	1.01E-39	1.33E-90	8.60E-136	2.2E-3
637 nm	6.12E-94	3.06E-43	9.74E-79	8.10E-161	2.2E-2

Table SI 5: Absorption coefficient multivariate regression p-values

	OOA-1	OOA-2	HOA	BBOA	BC	intercept
370 nm	1.8E-15	8.0E-04	1.6E-12	1.8E-132	0	3.6E-72
470 nm	3.26E-18	3.65E-04	1.11E-11	1.09E-104	0	6.91E-72
520 nm	7.28E-29	4.18E-04	2.03E-05	2.98E-88	0	7.30E-72
637 nm	1.66E-44	2.40E-05	0.661653	4.92E-55	0	1.18E-69
880 nm	2.10E-69	3.85E-20	1.61E-09	2.16E-18	0	7.84E-30

Reconstructed scattering and absorption coefficients from MLR method
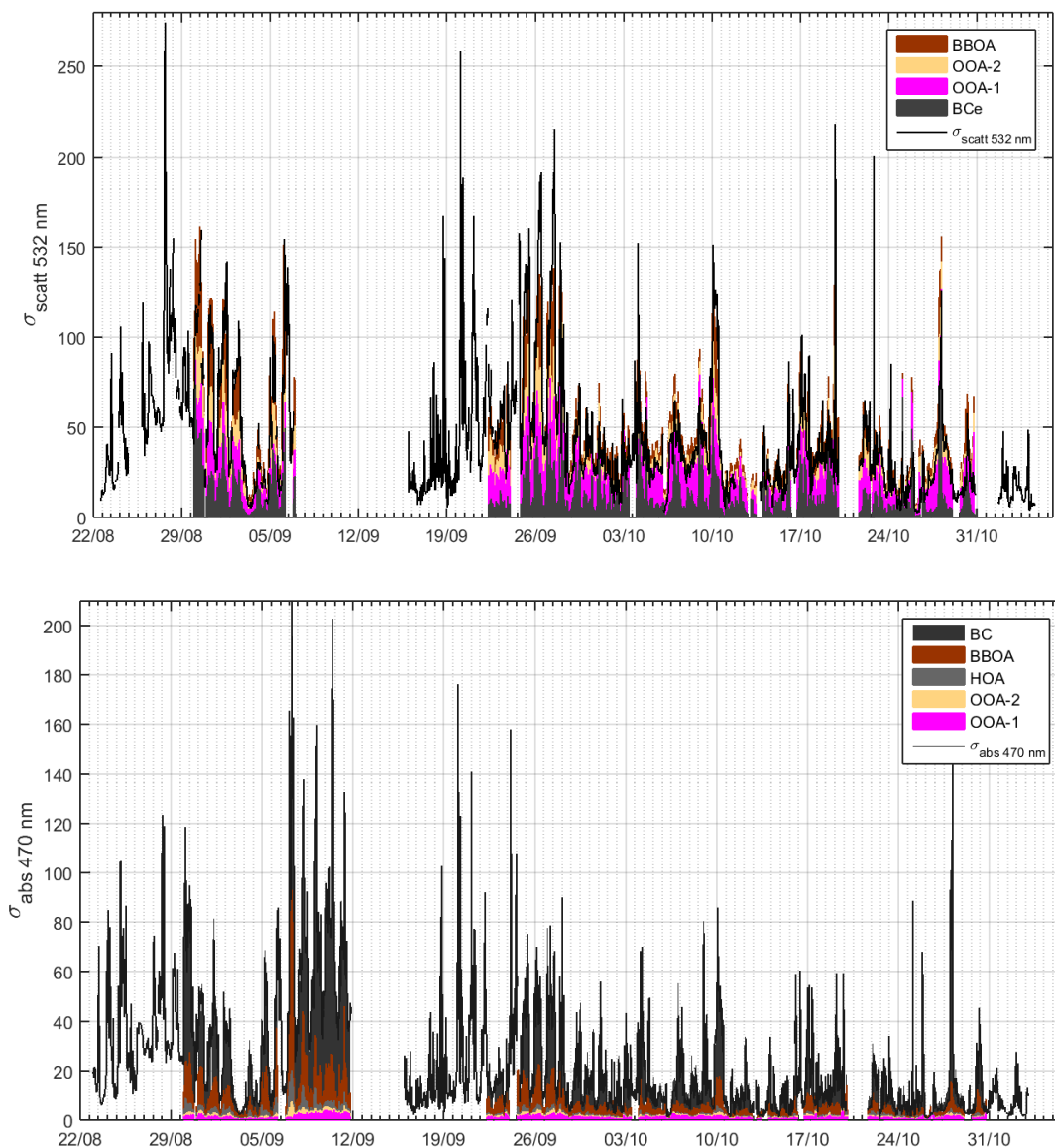
Figure SI 14 Time series of the reconstructed coefficients obtained from the linear model using OA PMF factors and BC compared to the measured data for a) scattering coefficient (σscat) for 532 nm. b) absorption coefficient (σabs) at 470 nm.

Org Absorption Coefficient vs BrC
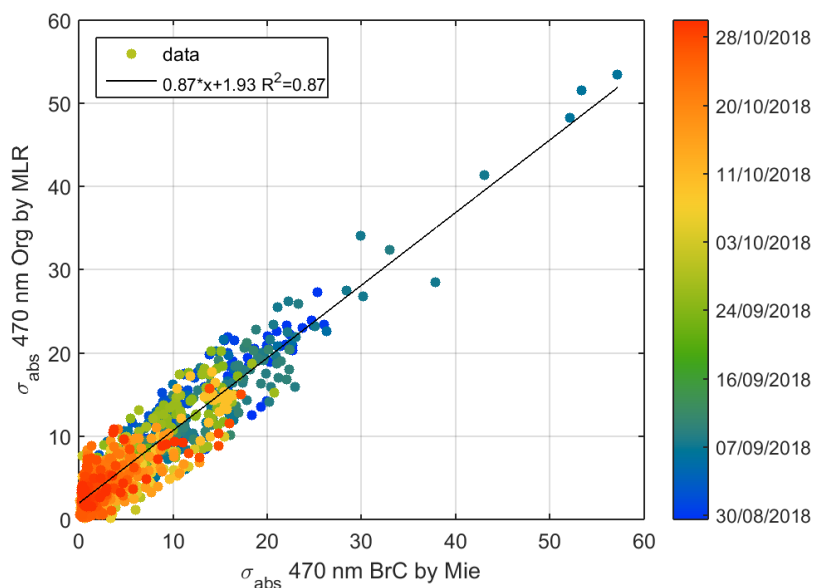
Figure SI 15: The contribution of total organics to the absorption coefficient compared to the contribution from BrC at 470 nm estimated from absorption spectra. p-value (for 95% CI) is 1.59 e^{-184}.

References

1   A. M. Yáñez-Serrano, A. C. Nölscher, J. Williams, S. Wolff, E. Alves, G. A. Martins, E. Bourtsoukidis, J. Brito, K. Jardine, P. Artaxo and J. Kesselmeier, Diel and seasonal changes of biogenic volatile organic compounds within and above an Amazonian rainforest, *Atmos. Chem. Phys.*, 2015, **15**, 3359–3378.

2   M. O. Andreae, P. Artaxo, C. Brandão, F. E. Carswell, P. Ciccioli, A. L. Da Costa, A. D. Culf, J. L. Esteves, J. H. C. Gash, J. Grace, P. Kabat, J. Lelieveld, Y. Malhi, A. O. Manzi, F. X. Meixner, A. D. Nobre, C. Nobre, M. D. L. P. Ruivo, M. A. Silva-Dias, P. Stefani, R. Valentini, J. Von Jouanne and M. J. Waterloo, Biogeochemical cycling of carbon, water, energy, trace gases, and aerosols in Amazonia: The LBA-EUSTACH experiments, *J. Geophys. Res. Atmos.*, , DOI:10.1029/2001JD000524.

3   I. Trebs, O. L. Mayol-Bracero, T. Pauliquevis, U. Kuhn, R. Sander, L. Ganzeveld, F. X. Meixner, J. Kesselmeier, P. Artaxo and M. O. Andreae, Impact of the Manaus urban plume on trace gas mixing ratios near the surface in the Amazon Basin: Implications for the NO-NO2-O 3 photostationary state and peroxy radical levels, *J. Geophys. Res. Atmos.*, 2012, **117**, 1–16.

4   J. P. Nascimento, M. M. Bela, B. B. Meller, A. L. Banducci, L. V. Rizzo, A. Liduvino Vara-Vela, H. M. J. Barbosa, H. Gomes, S. A. A. Rafee, M. A. Franco, S. Carbone, G. G. Cirino, R. A. F. Souza, S. A. Mckeen and P. Artaxo, Aerosols from anthropogenic and biogenic sources and their interactions-modeling aerosol formation, optical properties, and impacts over the central Amazon basin, *Atmos. Chem. Phys.*, 2021, **21**, 6755–6779.

5   F. Pacifico, G. A. Folberth, S. Sitch, J. M. Haywood, L. V. Rizzo, F. F. Malavelle and P. Artaxo, Biomass burning related ozone damage on vegetation over the Amazon forest: A model sensitivity study, *Atmos. Chem. Phys.*, 2015, **15**, 2791–2804.

6   J. Brito, L. V. Rizzo, W. T. Morgan, H. Coe, B. Johnson, J. Haywood, K. Longo, S. Freitas, M. O. Andreae and P. Artaxo, Ground-based aerosol characterization during the South American Biomass Burning Analysis (SAMBBA) field experiment, *Atmos. Chem. Phys.*, 2014, **14**, 12069–12083.